Induction of Colossal Magnetoresistance in the Double Perovskite Sr_2CoMoO_6

M. C. Viola,[†] M. J. Martínez-Lope,[‡] J. A. Alonso,*[,‡] P. Velasco,[‡] J. L. Martínez,[‡] J. C. Pedregosa,[†] R. E. Carbonio,[§] and M. T. Fernández-Díaz[||]

Area de Química General e Inorgánica "Dr. Gabino F. Puelles", Departamento de Química, Facultad de Química, Bioquímica y Farmacia, Universidad Nacional de San Luis, Chacabuco y Pedernera, 5700-San Luis, Argentina, Instituto de Ciencia de Materiales de Madrid, C.S.I.C., Cantoblanco, E−28049 Madrid, Spain, Instituto de Investigaciones en Físico Química de Córdoba (INFIQC), Departamento de Fisicoquímica, Facultad de Ciencias Químicas, Universidad Nacional de Córdoba, Ciudad Universitaria, 5000 Córdoba, Argentina, and Institut Laue-Langevin, B.P. 156, F-38042 Grenoble Cedex 9, France

Received July 20, 2001. Revised Manuscript Received October 8, 2001

Sr_2CoMoO_6 perovskite has been prepared in polycrystalline form by thermal treatment, in air, of previously decomposed citrate precursors. This material has been studied by X-ray (XRD) and neutron powder diffraction (NPD), thermal analysis, and magnetic, magnetotransport, and Hall effect measurements. At room temperature, the crystal structure is tetragonal with a space group $I4/m$, with $a = 5.565\ 03(5)$ and $c = 7.948\ 10(8)$ Å. The crystal contains alternating CoO_6 and MoO_6 octahedra, tilted by 6.8° in the basal *ab* plane. Magnetic measurements indicate an antiferromagnetic ordering below $T_N = 37$ K. As prepared, the sample is an electrical insulator. The topotactic reduction of the stoichiometric sample, in H_2/N_2 flows, leads to oxygen-deficient double perovskites, $Sr_2CoMoO_{6-\delta}$, $\delta = 0.03$ and 0.14. The magnetic behavior of the reduced samples suggests the presence of ferromagnetic domains characterized by Curie temperatures of $T_C = 350-370$ K. The conductivity dramatically increases upon H_2 reduction; the number of charge carriers, as determined by Hall effect measurements, are 1.7×10^{-7} and 6×10^{-6} electrons per unit cell for $\delta = 0.03$ and 0.14 samples, respectively. Moreover, the reduced samples exhibit colossal magnetoresistance, as high as 30% at 12 K for $H = 9T$. Magnetic and magnetotransport results are consistent with a large component of itinerancy for down-spin Mo t_{2g} electrons, injected through hydrogen reduction.

Introduction

The discovery of colossal magnetoresistance (CMR) properties in hole-doped manganese perovskites has stimulated the enthusiasm of solid-state chemists and physicists, since this effect is of technological interest for the detection of magnetic fields in magnetic memory devices.[1,2] CMR materials undergo a large change in electrical resistance in response to an external magnetic field. In these compounds, the applied field tends to align the local spins and hence leads to a rapid drop of the measured resistivity by suppressing spin fluctuations and enhancing electronic transfer. As basic features, a CMR material must exhibit a semimetallic, spin-polarized conductivity and experience a ferromagnetic (FM) ordering at Curie temperatures, T_C, as high as possible, ideally well above room temperature (RT). It is now well established that Curie temperatures of mixed-valence manganites (based upon $LaMnO_3$ perovskite) cannot be increased above 400 K by any chemical substitution. Materials with a substantially higher T_C must be developed to operate in an useful temperature range around RT.

Recently, some members of the family of double perovskites of composition $A_2B'B''O_6$ (A = alkali earths, B′, B″: transition metals) have been proposed as half-metallic ferromagnets (best described as ferrimagnets), with T_C's well above RT, as an alternative to perovskite manganites.[3−7] The revival of interest in this family was triggered by a report on Sr_2FeMoO_6,[3] demonstrating that in the electronic structure only minority spins are present at the Fermi level; this material was shown to exhibit intrinsic tunneling-type magnetoresistance (MR) at RT.[3,7] In a simple picture, FeO_6 and MoO_6 octahedra alternate along the three directions of the crystal

* To whom correspondence should be addressed.
[†] Universidad Nacional de San Luis.
[‡] Instituto de Ciencia de Materiales de Madrid.
[§] Universidad Nacional de Córdoba.
[||] Institut Laue-Langevin.

(1) Ramirez, A. P. *J. Phys: Condens. Matter* **1997**, *9*, 8171.
(2) *Colossal magnetoresistance and other related properties in 3d oxides*; Rao, C. N. R., Raveau, B., Eds.; World Scientific: Singapore, 1998.
(3) Kobayashi, K.-I.; Kimura, T.; Sawada, H.; Terakura, K.; Tokura, Y. *Nature* **1998**, *395*, 677.
(4) García-Landa, B.; Ritter, C.; Ibarra, M. R.; Blasco, J.; Algarabel, P. A.; Mahendiran, R.; García, J. *Solid State Commun.* **1999**, *110*, 435.
(5) Maignan, A.; Raveau, B.; Martin, C.; Hervieu, M. *J. Solid State Chem.* **1999**, *144*, 224.
(6) Kobayashi, K.-I.; Kimura, T.; Tomioka, Y.; Sawada, H.; Terakura, K.; Tokura, Y. *Phys. Rev. B* **1999**, *59*, 11159.
(7) Kim, T. H.; Uehara, M.; Cheong, S.-W.; Lee, S. *Appl. Phys. Lett.* **1999**, *74*, 1737.

10.1021/cm011186j CCC: $22.00
Published on Web 01/25/2002

structure of Sr_2FeMoO_6; the ferrimagnetic structure can be described as an ordered arrangement of parallel Fe^{3+} ($S = 5/2$) magnetic moments antiferromagnetically coupled with Mo^{5+} ($S = 1/2$) spins.

The occurrence of MR properties is a common feature in other members of the $A_2B'B''O_6$ family. The A = Ca and Ba analogues of the A_2FeMoO_6 were also found to exhibit semimetallic and ferrimagnetic properties.[5,8−10] Also, A_2FeReO_6 (A = Ca, Sr, Ba) present[11] a half-metallic ground state concomitant with the ferrimagnetic coupling of Fe^{3+} and Re^{5+} ($5d^2$, $S = 2/2$) magnetic moments and show MR at RT. Also, MR was described in double perovskites with other B′ cations different from Fe, for instance, Sr_2CrMoO_6, which is ferrimagnetic ($T_C = 450$ K) although it shows considerable site disorder.[12] These results are encouraging in the exploration of other prospective half-metallic compounds as MR materials with sufficiently large effect at low magnetic fields, in ferromagnets with T_C's as close as possible to RT.

The Co analogue of Sr_2FeMoO_6 has attracted our attention. The double perovskite Sr_2CoMoO_6 was first studied in the sixties.[13,14] It was reported to be an antiferromagnet with $T_N = 34$ K.[15,16] The structure was described as a tetragonal distortion of perovskite,[13] with unit cell parameters $a = b = 3.9367$ and $c = 3.9764$ Å, assuming a random distribution of Co and Mo atoms; the space group was not given. More recently, it has also been described as tetragonal, with doubled unit cell parameters ($a = b \approx c \approx 2a_0$), in the space group $I4/mmm$.[17]

In the present work, we describe the synthesis of this material, prepared by "chimie douce" procedures, and the results of a neutron powder diffraction (NPD) study on a well-crystallized Sr_2CoMoO_6 sample. The structure has been revisited; we report complete structural data for this tetragonally distorted perovskite, which contains two crystallographically independent sites for Co and Mo cations. Most interestingly, we describe the dramatic changes experienced by the magnetic and transport properties upon controlled H_2 reduction, which leads to the induction of CMR properties comparable to those described for Sr_2FeMoO_6.

Experimental Section

The oxygen-stoichiometric Sr_2CoMoO_6 perovskite was prepared as a black polycrystalline powder from citrate precursors obtained by soft chemistry procedures. Stoichiometric amounts of analytical grade $Sr(NO_3)_2$, $Co(NO_3)_2{\cdot}6H_2O$, and $(NH_4)_6Mo_7O_{24}{\cdot}\ 4H_2O$ were dissolved in citric acid. The citrate + nitrate solutions were slowly evaporated, leading to organic resins containing a random distribution of the involved cations at an atomic level. These resins were first dried at 120 °C and then slowly decomposed at temperatures up to 600 °C. All the organic materials and nitrates were eliminated in a subsequent treatment at 800 °C in air, for 2 h. This treatment gave rise to highly reactive precursor materials. Afterward, the resulting black powder was treated at 1150 °C in air for 24 h.

The oxygen-deficient $Sr_2CoMoO_{6-\delta}$ perovskites were prepared by topotactic reduction of the oxygen-stoichiometric perovskite in an H_2/N_2 flow at 850 °C for 2 h. Two different H_2 concentrations were used (5 and 15%), leading to two different oxygen-deficient samples labeled R5 and R15, respectively, with different δ values. These values were subsequently determined by thermal analysis in an air flow. Thermal treatments longer than 2 h did not result in increased δ values, suggesting that the nonstoichiometric phases reach an equilibrium with the atmosphere after this treatment time, in such a way that δ is determined only by the annealing temperature and H_2 concentration. For the resistivity, Hall, and magnetotransport measurements, R5 and R15 powder samples were pressed in bar-shaped pellets and sintered at 850 °C for 2 h in 5 and 15% H_2/N_2 flow, respectively.

The initial characterization of the products was carried out by laboratory X-ray diffraction (XRD) measurements (Cu Kα, $\lambda = 1.5418$ Å). For the structural refinements, RT NPD patterns of stoichiometric Sr_2CoMoO_6 and the reduced R15 sample were collected at the high-resolution D2B neutron diffractometer of ILL-Grenoble. The high-flux mode was used. About 8 g of sample was contained in a vanadium can; the counting time was 3 h. A wavelength of 1.594 Å was selected from a Ge monochromator. The patterns were refined by the Rietveld method by using the FULLPROF refinement program.[18] A pseudo-Voigt function was chosen to generate the line shape of the diffraction peaks. The minor $SrMoO_4$ impurity was included as a second crystallographic phase in the refinements. In the final runs, the following parameters were refined: scale factors for the main and impurity phases, background coefficients, zero-point error, unit cell parameters, pseudo-Voigt corrected for asymmetry parameters, positional coordinates, anisotropic thermal factors, and antisite disorder of Co/Mo. The coherent scattering lengths for Sr, Co, Mo, and O were, 7.02, 2.49, 6.72, and 5.803 fm, respectively.

Thermal analysis of the reduced samples was performed in a Mettler TA3000 system equipped with a TC10 processor unit. Thermogravimetric (TG) curves were obtained in a TG50 unit, working at a heating rate of 5 °C min^{-1}, in an air flow of 0.3 l min^{-1}. About 30 mg of the sample was used in each experiment**.** The dc and ac magnetic susceptibilities were measured with a commercial SQUID magnetometer on powdered samples, in the temperature range of 1.7−400 K; transport and magnetotransport measurements were performed by the conventional four probe technique, under magnetic fields up to 9 T in a PPMS system from Quantum Design, in sintered pellets of $10 \times 3 \times 2$ mm^3. The Hall effect was measured in the Hall-bar configuration, up to $H = 9$ T.

Results

Sr_2CoMoO_6 and $Sr_2CoMoO_{6-\delta}$ were obtained as black, well-crystallized powders. The laboratory XRD diagrams of the stoichiometric compound, obtained in air, and the reduced R15 sample are shown in Figure 1. Both patterns are characteristic of a perovskite structure, showing superstructure peaks corresponding to the Co/Mo ordering and the splitting of certain reflections, characteristic of a tetragonal distortion (for instance, (004) and (220) reflections). Minor amounts of $SrMoO_4$

(8) Alonso, J. A.; Casais, M. T.; Martínez-Lope, M. J.; Velasco, P.; Muñoz, A.; Fernández-Díaz, M. T. *Chem. Mater.* **2000**, *12*, 161.
(9) Borges, R. P.; Thomas, R. M.; Cullinan, C.; Coey, J. M. D.; Suryanarayan, R.; Ben-Dor, L.; Pinsard-Gaudart, L.; Revcolevschi, A. *J. Phys.: Condens. Matter* **1999**, *11*, L445.
(10) Ritter, C.; Ibarra, M. R.; Morellón, L.; Blasco, J.; García, J.; De Teresa, J. M. *J. Phys.: Condens. Matter* **2000**, *12*, 8295.
(11) Prellier, W.; Smolyaninova, W.; Bisbas, A.; Galley, C.; Greene, R. L.; Ramesha, K.; Gopalakrishnan, J. *J. Phys.: Condens. Matter* **2000**, *12*, 965.
(12) Arulraj, A.; Ramesha, K.; Gopalakrishnan, J.; Rao, C. N. R. *J. Solid State Chem.* **2000**, *155*, 233.
(13) (a) Galasso, F. *Structure, Properties and Preparation of Perovskite-Type Compounds*; Pergamon Press: Oxford, 1969. (b) Brixner, L. *J. Phys. Chem.* **1960**, *64*, 165.
(14) Kupriyanov, M. F.; Fesenko, E. G. *Sov. Phys. Crystallogr.* **1962**, *7*, 358.
(15) Landolt-Börnstein. *Zahlenwerte und Funktionen aus Naturwissenschaften und Tecnik* (Neue serie, Band 4, Teil a); Springer-Verlag: Berlin, 1970.
(16) Blasse, G. *Bull. Soc. Chim. Fr.* **1965**, 1212.
(17) Morimoto, Y.; Xu, Sh.; Machida, A.; Akimoto, T.; Nishibori, E.; Takata, M.; Sakata, M. *Phys. Rev. B* **2000**, *61*, R7827.
(18) Rodríguez-Carvajal, J. *Physica B (Amsterdam)* **1993**, *192*, 55.

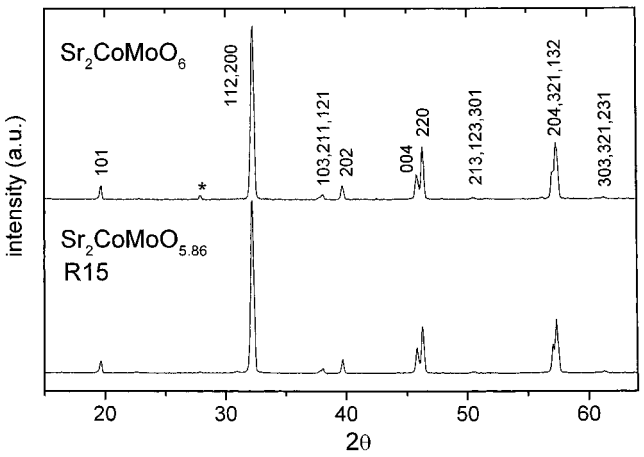

Figure 1. XRD patterns for Sr_2CoMoO_6 (stoichiometric and R15 samples), indexed in a tetragonal unit cell with $a = b \approx (2a_0)^{1/2}$, $c \approx 2a_0$, and $a_0 \approx 3.9$ Å. The star indicates the most intense reflection of the $SrMoO_4$ impurity phase.

were detected from either XRD or NPD data. For the reduced samples, the topotactic removal of oxygen atoms leads to an oxygen-deficient perovskite in which the crystal structure undergoes very subtle modifications. In the XRD pattern of the R15 sample (Figure 1), there are no apparent changes or additional impurity phases, and the unit cell parameters differ in the third decimal place from those of the stoichiometric sample.

Structural Refinement. For the stoichiometric Sr_2CoMoO_6 and the reduced R15 perovskites, the structural refinement from RT high-resolution NPD data was performed in the $I4/m$ space group (No. 87), $Z = 2$, with unit cell parameters related to a_0 (ideal cubic perovskite, $a_0 \approx 3.9$ Å) as $a = b \approx (2a_0)^{1/2}$ and $c \approx 2a_0$. Sr atoms were located at 4d positions, Co at 2a, Mo at 2b sites, and oxygen atoms at 4e and 8h positions. $SrMoO_4$ was included in the refinement as a second phase, defined[19] in the space group I_1/a (1.6% of this phase from the scale factors, for both samples). An excellent fit was obtained for this model, as illustrated in Figure 2 for Sr_2CoMoO_6. In the final refinement, the possibility of antisite disordering was checked by assuming that some Co atoms could occupy Mo sites and vice versa: the refinement of the inversion degree led to less than 2% of antisite disordering in both the stoichiometric Sr_2CoMoO_6 and the reduced R15 sample. Notice that the unit cell of R15 is slightly expanded with respect to the stoichiometric sample, corresponding to the partial reduction of the transition-metal cations. Table 1 includes the final atomic coordinates and agreement factors after the refinement. Table 2 lists the main interatomic distances and angles.

Thermal Analysis of the Reduced Samples. The reduced samples are stable in an air flow up to 580 °C; above this temperature, an oxidation process starts which leads back to the stoichiometric Sr_2CoMoO_6 perovskite. Figure 3 illustrates this process for the R15 sample. The weight gain corresponds to the incorporation of 0.03 oxygen atoms per formula for R5 and 0.14 oxygen atoms per formula for R15. Thus, the stoichiometries of the reduced samples are $Sr_2CoMoO_{5.97}$ and $Sr_2CoMoO_{5.86}$ for R5 and R15, respectively.

Magnetic Data. The magnetic susceptibility vs temperature data for the stoichiometric Sr_2CoMoO_6 perovskite (Figure 4) shows a low-temperature maximum, at $T_N = 37$ K, corresponding to the transition to an antiferromagnetically ordered phase. A similar Néel temperature (34 K) had been reported for this com-

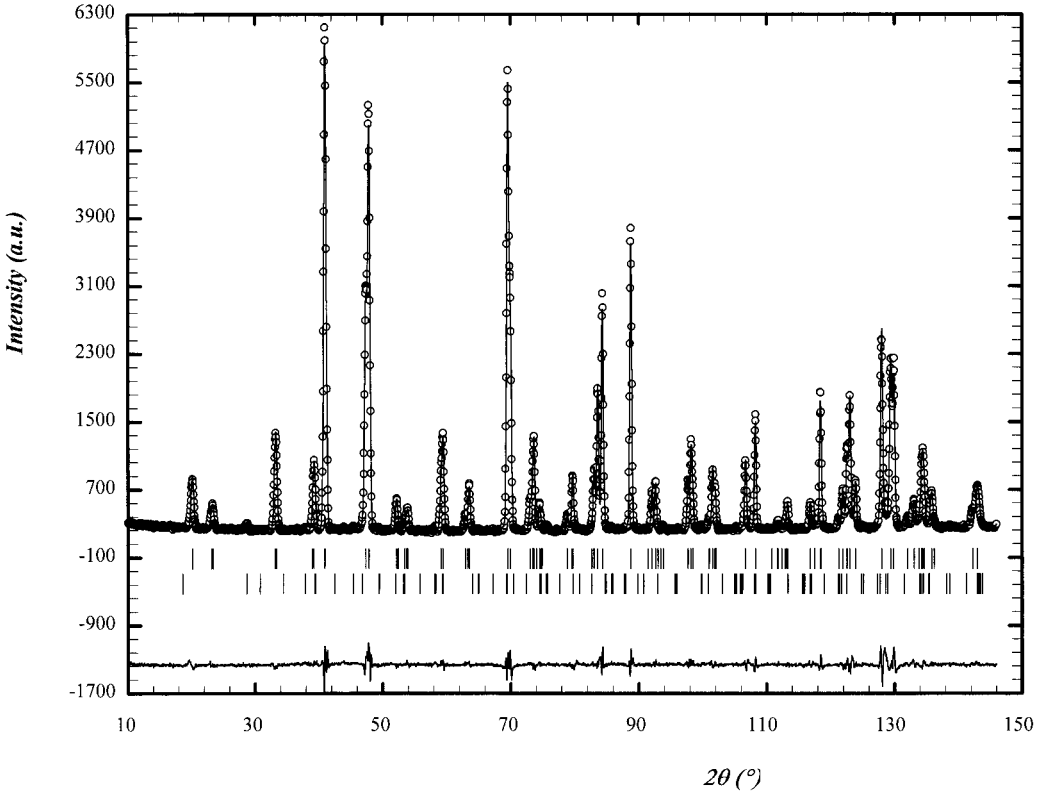

Figure 2. Observed (circles), calculated (full line), and difference (bottom) NPD Rietveld profiles for stoichiometric Sr_2CoMoO_6 at 295 K. The second series of tick marks correspond to the Bragg reflections of the $SrMoO_4$ impurity phase.

Table 1. Positional and Anisotropic Thermal Parameters for Sr_2CoMoO_6 in the Tetragonal *I4/m* Space Group, $Z = 4$, from NPD Data at 295 K. Reliability Factors after the Rietveld Refinement are Also Given

(a) Stoichiometric Sample: The Unit Cell Parameters Are $a = b = 5.565\ 03(5)$ Å, $c = 7.948\ 10(8)$ Å, and $V = 246.149(4)$ Å^3

atom	site	*x*	*y*	*z*	$\beta_{11} \times 10^4$	$\beta_{22} \times 10^4$	$\beta_{33} \times 10^4$	$\beta_{12} \times 10^4$	$\beta_{13} \times 10^4$	$\beta_{23} \times 10^4$
Sr	4d	0	0.5	0.25	54(2)	54(2)	35(2)	0	0	0
Co	2a	0	0	0	53(18)	53(18)	45(9)	0	0	0
Mo	2b	0	0	0.5	17(6)	17(6)	6(3)	0	0	0
O1	4e	0	0	0.2589(3)	103(3)	103(3)	23(2)	0	0	0
O2	8h	0.2895(3)	0.2296(3)	0	56(5)	34(5)	60(1)	−25(3)	0	0

discrepancy factors: $R_p = 3.79\%$, $R_{wp} = 5.06\%$, $R_{exp} = 2.74\%$, $\chi^2 = 3.41$, $R_I = 2.02\%$

(b) Reduced R15 Sample: The Unit Cell Parameters Are $a = b = 5.568\ 41(4)$ Å, $c = 7.954\ 36(6)$ Å, and $V = 246.642(3)$ Å^3

atom	site	*x*	*y*	*z*	$\beta_{11} \times 10^4$	$\beta_{22} \times 10^4$	$\beta_{33} \times 10^4$	$\beta_{12} \times 10^4$	$\beta_{13} \times 10^4$	$\beta_{23} \times 10^4$
Sr	4d	0	0.5	0.25	59(2)	59(2)	31(2)	0	0	0
Co	2a	0	0	0	49(18)	49(18)	43(10)	0	0	0
Mo	2b	0	0	0.5	20(6)	20(6)	5(3)	0	0	0
O1	4e	0	0	0.2588(3)	109(3)	109(3)	20(2)	0	0	0
O2	8h	0.2901(3)	0.2300(3)	0	58(5)	43(5)	55(1)	−27(3)	0	0

discrepancy factors: $R_p = 2.99\%$, $R_{wp} = 3.98\%$, $R_{exp} = 3.04\%$, $\chi^2 = 1.71$, $R_I = 1.92\%$

Table 2. Main Bond Distances (Å) and Selected Angles (deg) for Tetragonal Sr_2CoMoO_6 Determined from NPD Data at 295 K

(a) Stoichiometric Sample		(b) Reduced R15 Sample	
CoO_6 octahedron		CoO_6 octahedron	
Co−O1 (×2)	2.057(3)	Co−O1 (×2)	2.059(3)
Co−O2 (×4)	2.056(1)	Co−O2 (×4)	2.061(2)
⟨Co−O⟩	2.056(2)	⟨Co−O⟩	2.060(2)
MoO_6 octahedron		MoO_6 octahedron	
Mo−O1 (×2)	1.917(3)	Mo−O1 (×2)	1.918(3)
Mo−O2 (×4)	1.907(1)	Mo−O2 (× 4)	1.904(2)
⟨Mo−O⟩	1.910(2)	⟨Mo−O⟩	1.909(2)
Co−O1−Mo (×2)	180.0	Co−O1−Mo (×2)	180.0
Co−O2−Mo (×4)	166.30(6)	Co−O2−Mo (×4)	166.26(6)
SrO_{12} polyhedron		SrO_{12} polyhedron	
Sr−O1 (×4)	2.7834(1)	Sr−O1 (×4)	2.7851(1)
Sr−O2 (×4)	2.968(1)	Sr−O2 (×4)	2.971(1)
Sr−O2 (×4)	2.637(1)	Sr−O2 (×4)	2.638(1)
⟨Sr−O⟩	2.796(1)	⟨Sr−O⟩	2.798(1)

pound.[17] The reciprocal susceptibility data above T_N show a slight curvature, probably due to crystal field effects or a progressive change in the population of the low-spin vs high-spin electronic configurations for Co cations. A temptative Curie−Weiss fit above 200 K gives a paramagnetic moment of 5.3 μ_B/f.u., which is much larger than expected for spin only Co^{2+}/Mo^{6+} (in any spin configuration for Co^{2+}). This point will be discussed in detail.

The susceptibility curves of the reduced samples, R5 and R15, shown in parts a and b of Figure 5, are surprising. They present a high-temperature transition

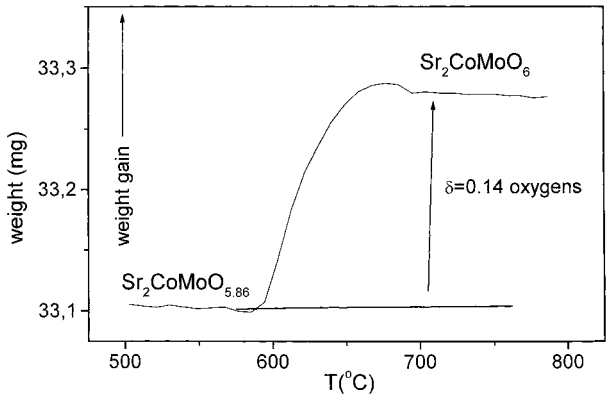

Figure 3. TG curve of the R15 sample, obtained in an air flow at 10 °C min^{-1}.

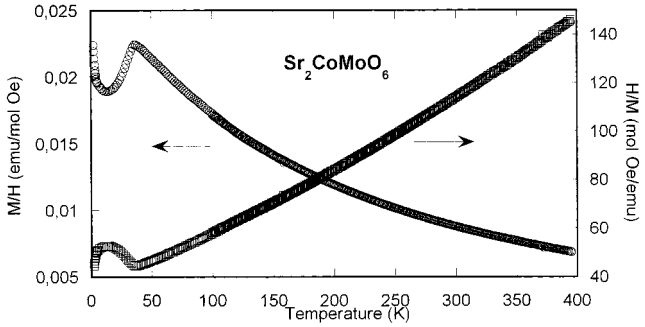

Figure 4. Temperature dependence of the dc magnetic susceptibility and the reciprocal susceptibility of Sr_2CoMoO_6.

consisting of an abrupt susceptibility increase, reminiscent of a partial FM ordering at $T_C = 350$ K for R5 and $T_C = 370$ K for R15. Also, there is a progressive increase of the susceptibility level from the stoichiometric sample to R5 and R15, as shown in the inset of Figure 5b. Notice that the maxima corresponding to the antiferromagnetic (AF) ordering at $T_N = 37$ K are also present, although much weaker, in the R5 and R15 curves. The dominant FM character of the transitions observed above RT is clearly appreciated at the magnetization isotherms shown in Figure 6. A linear behavior is observed for the stoichiometric Sr_2CoMoO_6 perovskite in the *M* vs *H* curves, as expected for a pure antiferromagnet; however, an extra magnetization is induced by the magnetic field for R5 and R15, although the saturation is not reached for fields up to 6 T: the magnetizations, extrapolated to zero field, are 0.054(1) and 0.192(1) μ_B/f.u. for R5 and R15, respectively. This behavior is characteristic of a weak ferromagnet or a canted antiferromagnet, where both AF and FM interactions are present, or in any case suggests the presence of FM domains imbedded in a predominant AFM matrix.

Transport and Magnetotransport. The resistivity of the stoichiometric Sr_2CoMoO_6 perovskite resulted in being too high to be measured (above 10^8 ohms at RT); this compound must be considered as an insulator. Conversely, the reduced samples show much lower resistivities, as shown in Figure 7; at RT, the resistivi-

(19) Guermen, E.; Daniels, E.; King, J. S. *J. Chem. Phys.* **1971**, *55*, 1093.

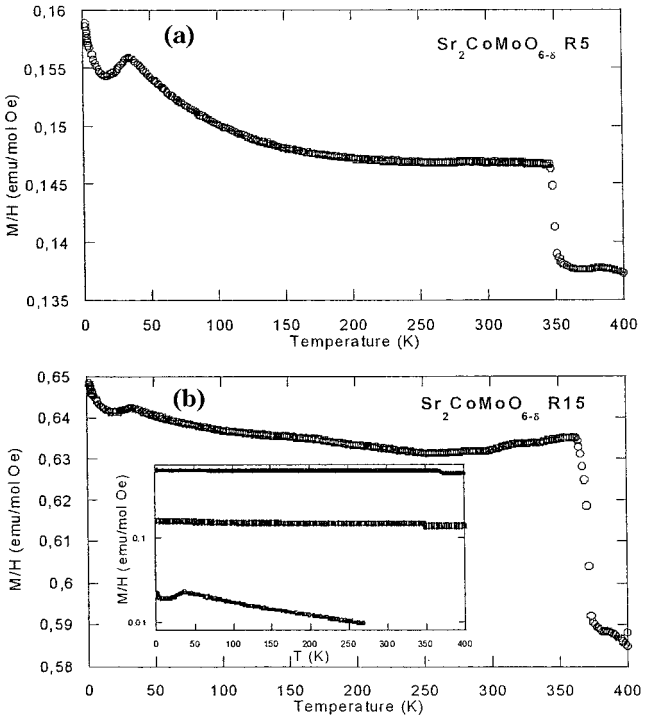

Figure 5. Magnetic susceptibility for (a) R5 and (b) R15 samples. The inset shows the relative magnitude of the susceptibilities for the stoichiometric and reduced R5 and R15 samples.

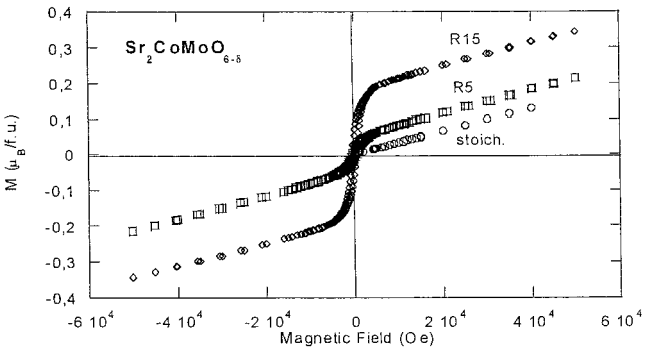

Figure 6. Magnetization vs field isotherms ($T = 5$ K) for the stoichiometric and reduced R5 and R15 samples.

ties of R5 and R15 are 80 and 12 Ωcm, respectively. The resistivities increase exponentially at lower temperatures, showing a semiconducting-like or thermally activated behavior. Hall coefficient measurements performed on the reduced samples demonstrate that at 200 K, the carriers involved in the conduction process are electrons and the number of charge carriers per unit cell is 1.7×10^{-7} and 6×10^{-6} for the R5 and R15 samples, respectively.

The variation of the electrical resistivity under a magnetic field is illustrated in the magnetotransport isotherms shown in parts a and b of Figure 8. The magnetoresistance, defined as $\mathrm{MR}(H) = 100 \times [R(0) - R(H)/R(0)]$, regularly increases as temperature diminishes. MR(9 T) reaches values higher than 25% at 12 K for R5 and close to 5% for R15 at 2 K, under fields of 9 T.

Discussion

The perovskite structure ABO_3 consists of a three-dimensional framework of vertex-sharing BO_6 octahedra, the voids of which are occupied by the more voluminous A cations. When A decreases in size, BO_6 octaedra tilt to optimize A−O distances. The 23 different octahedral tilting systems were originally studied by Glazer[20] and later on by O'Keeffe and Hyde.[21] More

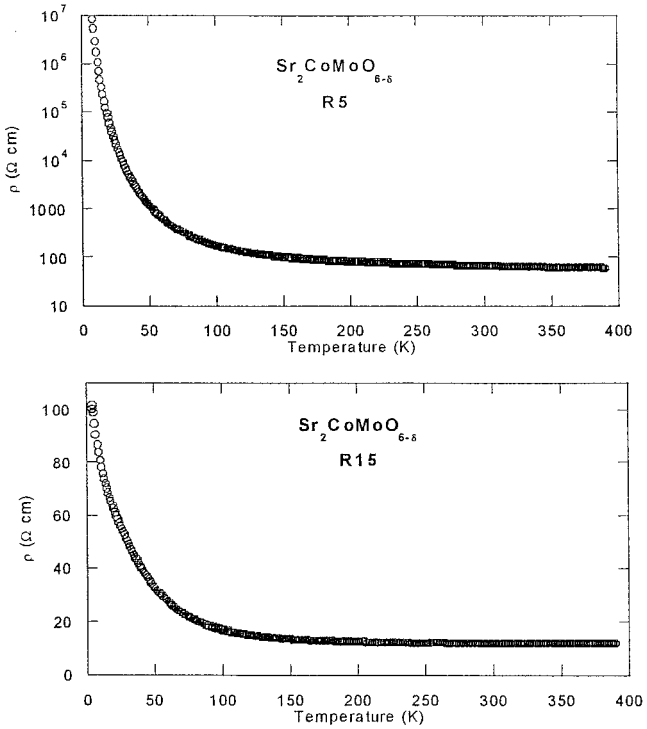

Figure 7. Resistivity vs temperature curves for R5 and R15 reduced samples.

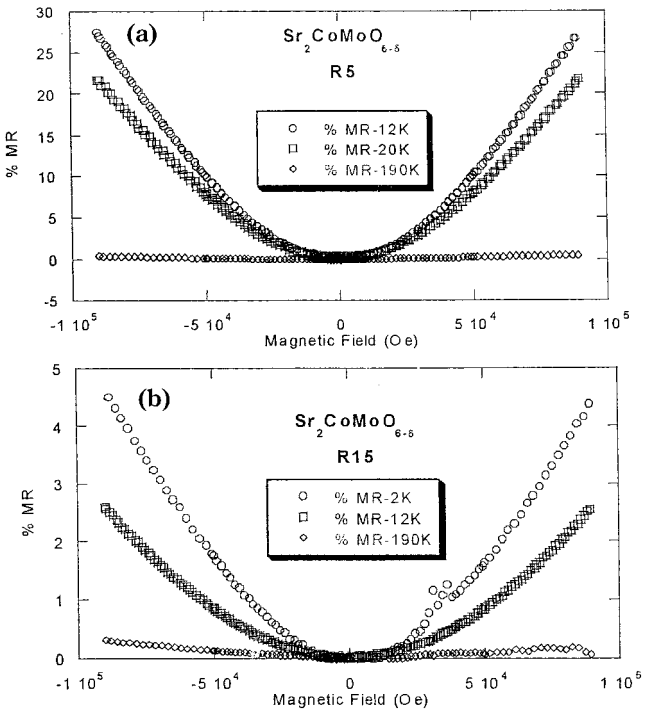

Figure 8. Magnetoresistance isotherms at selected temperatures for (a) R5 and (b) R15. Magnetoresistance is defined as $\mathrm{MR} = 100 \times [R(0) - R(H)]/R(0)$. The oxygen-stoichiometric sample was found to be an insulator; thus, R and MR could not be measured.

(20) Glazer, A. M. *Acta Crystallogr., Sect. B* **1972**, *28*, 3384.

recently, Woodward[22] has described the possible tilting systems for $A_2B'B''O_6$-ordered perovskites, predicting the space groups for each system. When A cation is large enough, the well-known $(NH_4)_3FeF_6$ structure is adopted by 1:1 B-site-ordered perovskites, such as Ba_2FeMoO_6, which can be described in the cubic space group $Fm\bar{3}m$. For slightly smaller A cations, only a small deformation of the lattice takes place, implying the tilting of the octahedra only along the *c* axis. This tilting means a reduction in symmetry from cubic to tetragonal. Depending on the sign of the tilt, either in phase ($a^0a^0a^+$ according to the Glazer's nomenclature[20]) or antiphase ($a^0a^0c^-$), two space groups describe the changes in symmetry: $P4/mnc$ in the first case or $I4/m$ in the second one.

The difference between both models is very subtle, since it mainly involves small shifts of the in-plane oxygen atoms. These position changes can be difficult to detect by XRD; hence, a NPD study is essential to investigate these structural features, with neutrons being more sensitive to the oxygen positions. Our NPD study allowed us to determine the true space group at RT; a trial refinement in $P4/mnc$ led to a much worse fit of the data. Also, the space group $I4/mmm$ suggested by Morimoto et al.[17] was tried and rejected; this space group imposes a restriction for O2 positions (at 8*h*, (*x*, *x*, 0) site) leading to very bad agreement factors (R_{wp} = 22.4%, R_I = 12.6%) and abnormally high thermal factors for O2. Thus, the structure of Sr_2CoMoO_6 can be described in the $I4/m$ space group as the result of a single antiphase octahedral tilting along the *c* axis. Figure 9 illustrates this particular feature. The magnitude of the tilting can be simply derived from the Co−O2−Mo angle to be 6.8° at RT. CoO_6 and MoO_6 octahedra are almost fully ordered and alternate along the three directions of the crystal, in such a way that each CoO_6 octahedra is linked to six MoO_6 octahedra and vice versa, as shown in Figure 9.

The driving force for the Co/Mo ordering is the charge difference between both kinds of cations, since the size difference is not too large. In Table 2, we notice that MoO_6 octahedra are slightly larger (expanded) than CoO_6 octahedra. MoO_6 octahedra are slightly elongated along the *c* axis, whereas CoO_6 octahedra can be considered as regular, within the standard deviations.

The oxygen-stoichiometric Sr_2CoMoO_6 perovskite has been prepared in air, in such a way that, from the chemical point of view, an hexavalent oxidation state is expected for Mo cations with Co cations being divalent. The electronic configuration for this sample is $Co^{2+}(3d^7)-Mo^{6+}(4d^0)$, which also accounts for the electrical insulator behavior. This configuration requires a completely unquenched orbital contribution for the high-spin Co^{2+} cation, which explains the large effective moment obtained in the paramagnetic region, well above T_N, of 5.3 μ_B. Recently, V. Primo-Martín et al.[23] studied the $Sr_3CoSb_2O_9$ double perovskite, with an effective moment of 5.39 μ_B/f.u., and proposed a high-spin Co^{2+} configuration with completely unquenched orbital contribution ($^4T_{1g}$ term). This is not an isolated observation; many Co^{2+} compounds show effective moments between 3.87 μ_B (spin only) and 5.20 μ_B (spin plus completely unquenched orbital contribution);[24,25] some examples are CoF_2 (μ_{eff} = 5.15 μ_B) or CoO (μ_{eff} = 5.1 μ_B). The proposal by Morimoto et al.,[17] who considered an electronic configuration $Co^{III}(3d^6)-Mo^{5+}(4d^1)$, is hardly compatible with the synthesis in air and would suggest the presence of ferrimagnetic interactions and metallic behavior, which is not observed.

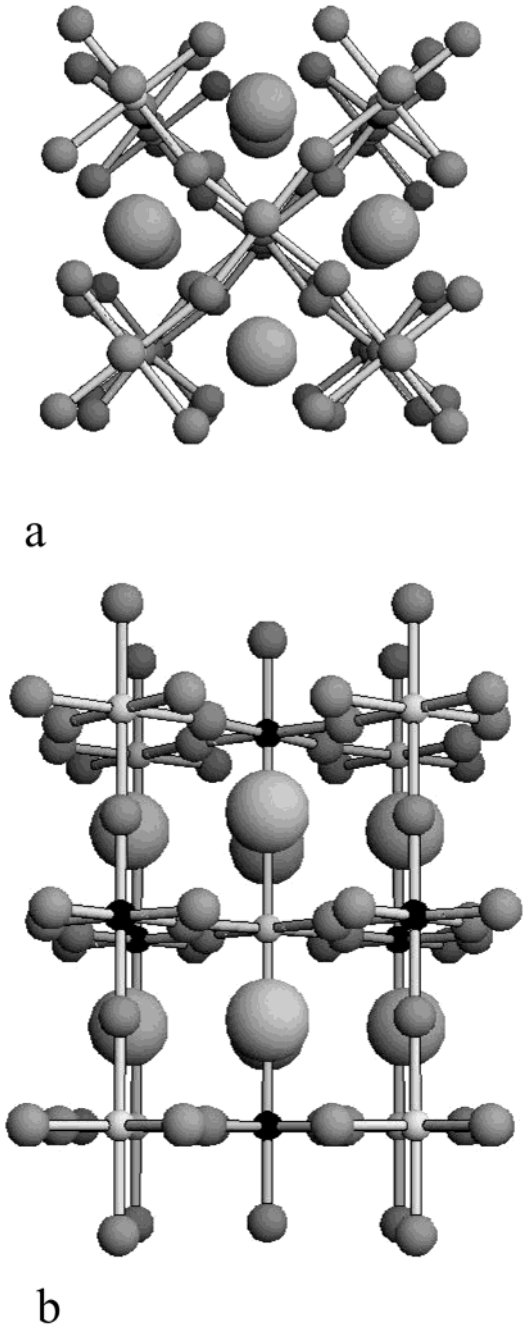

Figure 9. Two views of the structure of tetragonal Sr_2CoMoO_6: (a) along the *c* axis; (b) with the *c* axis vertical and the *a* axis from right to left. Large spheres represent Sr; corner-sharing CoO_6 (dark) and MoO_6 octahedra are tilted in antiphase along the *c* axis to optimize Sr−O bond lengths.

(21) O'Keeffe, M.; Hyde, B. G. *Acta Crystallogr., Sect. B* **1977**, *33*, 3802.
(22) Woodward, P. M. *Acta Crystallogr., Sect. B* **1997**, *53*, 32.
(23) Primo-Martín, V.; Jansen, M. *J. Solid State Chem.* **2001**, *157*, 76.
(24) Radwanski, R. J.; Ropka, Z. *Physica B* **2000**, *281/282*, 507.
(25) Mahendra, A.; Khan, D. C. *Phys. Rev. B* **1971**, *4*, 3901.

Regarding the electronic configurations of the B cations, the comparison with Sr_2FeMoO_6 is enlightening; although the actual electronic configurations $Fe^{3+}(3d^5)-Mo^{5+}(4d^1)$ vs $Fe^{2+}(3d^6)-Mo^{6+}(4d^0)$ have been considered as possible, the average valence for Fe has been found to be intermediate between high-spin configuration values of Fe^{2+} and Fe^{3+} from Mössbauer spectroscopy studies.[22] This is to say that both electronic configurations (with Fe^{2+} and Fe^{3+}) must be considered as degenerate, the final state being a combination of both configurations. The case of the stoichiometric Sr_2CoMoO_6 is very different; the electronic configuration $Co^{2+}(3d^7)-Mo^{6+}(4d^0)$ excludes the presence of mixed valence for Co, and there is no dynamic electron transfer between Co and Mo cations; i.e., the electrons are localized on the Co positions.

However, the reduction process to give $Sr_2CoMoO_{6-\delta}$ introduces, nominally, 2δ extra electrons that can partially occupy hybridized Mo 4d t_{2g} and Co 3d t_{2g} states. Nominally, a mixed $Mo^{6+}-Mo^{5+}$ valence state would be expected to take place for the reduced samples. The extra Mo electrons are responsible, as shown for Sr_2FeMoO_6, for the dramatic enhancement of the electronic conductivity, which increases with δ from R5 to R15, and for the FM interactions via superexchange between Co^{2+} and Mo^{5+} moments. The coexistence of important electronic conductivity and FM interactions below T_C accounts for the magnetotransport properties, as observed in other half-metallic FM double perovskites. In the absence of band-structure calculations, we can speculate that the extra itinerant Mo electrons occupy down-spin bands and they are shared among Co and Mo sites.

Nevertheless, the parallelism with Sr_2FeMoO_6 is not complete, because there is a significant difference with the $Sr_2CoMoO_{6-\delta}$ system; the necessary electrons have been introduced by chemical reduction through the introduction of oxygen vacancies. Taking into account the small number of introduced electrons, Mo^{5+} cations are isolated (probably at random) and the superexchange does not affect the integrity of the solid; only isolated clusters are formed, explaining the low saturation moments observed. On one hand, the introduction of oxygen vacancies are in the origin of the FM behavior, due to the concomitant introduction of extra electrons in the system, but, at the same time, the physical absence of these oxygens hinders the establishment of an homogeneous FM state, disturbing both the superexchange Co−O−Mo interactions and the electronic conduction paths. Instead of an homogeneous FM ground state, the formation of FM clusters in a paramagnetic matrix (or AFM matrix below T_N) would account for the observed low saturation moments.

The measured MR would be a result of the spin-dependent scattering of the charge carriers through the FM clusters; this scattering is reduced when an external magnetic field is applied thus aligning the orientation of the isolated clusters. The observed decay of MR with increasing temperature is comparable to that exhibited in other double perovskites, namely, Sr_2FeMoO_6, in which the main component of MR is attributable to grain boundary tunneling effects that take place at temperatures well below T_C.[3] This behavior is in contrast with that described in hole-doped manganese perovskites, in which a maximum in MR is observed at temperatures close to T_C, due to the intragranular or intrinsic character of this effect. On the other hand, it is remarkable that the MR for the R5 sample is considerably higher than that observed for R15. Majumdar and Littlewood[26] showed that MR in a wide variety of FM semimetals scales with the reciprocal of the number of charge carriers according to the expression $\Delta\rho/\rho = C(M/M_s)^2$, where $\Delta\rho/\rho$ is the MR, M and M_s are the magnetization and saturation magnetization of the sample, and C is a constant proportional to $n^{-2/3}$. According to this model, the MR can be tuned by properly modifying the carrier density of a given material; enhanced MR properties should be found in FM semimetals with a conveniently small number of carriers. Our results can be understood in the framework of this model, predicting an enhanced MR in a system with a lower number of charge carriers. Resistivity, magnetoresistivity, and Hall measurements consistently show a net increase of the number of free carriers upon oxygen removal in the $Sr_2CoMoO_{6-\delta}$ system.

Conclusions

Sr_2CoMoO_6 perovskite is an insulating antiferromagnet (T_N = 37 K), which can be converted into a semiconducting ferromagnet (T_C = 350−370 K) upon chemical reduction, via topotactic removal of oxygen atoms. The three members of the $Sr_2CoMoO_{6-\delta}$ series (δ = 0, 0.03, 0.14) adopt a tetragonal (space group $I4/m$) structure; the crystal contains alternating CoO_6 and MoO_6 octahedra, tilted in antiphase within the ab plane (Glazer notation $a^0a^0c^-$), as shown from NPD data for the $\delta = 0$ and 0.14 material at RT. Hall effect measurements demonstrate a dramatic increase in the number of carriers upon H_2 reduction, concomitant with a decrease in resistivity. The most remarkable result is the induction of MR, as high as 30% at 12 K for $H = 9$ T; the observed MR scales with the reciprocal of the number of charge carriers, as predicted by a model[26] that explains MR as a result of the scattering of a low-density electron gas by spin fluctuations concomitant with the FM long-range ordering or local spin bags of the magnetic cations. This picture is consistent with the magnetization results of the oxygen-defective samples, suggesting the presence of FM clusters imbedded in a AFM matrix.

Acknowledgment. We thank the financial support of CICyT to the projects MAT2001-0539 and MAT99-1045, and we are grateful to ILL for making all facilities available. J.C.P., M.C.V., and R.E.C. acknowledge the financial support of the Consejo Nacional de Investigaciones Cientificas y Técnicas (CONICET PID 4929/96 and PIP 380/98), the Agencia Nacional de Promoción Científica y Tecnológica (PICT98 06-03041 and PICT99 12-5378), Fundación Antorchas (collaboration project A-13740/1-94), CyT (Universidad Nacional de San Luis -Project 7707), and SECyT-UNC.

CM011186J

(26) Majumdar, P.; Littlewood, P. B. *Nature* **1998**, *395*, 479.